Classification
Physics Abstracts
6.350 — 7.130

POISEUILLE FLOW IN NEMATICS : EXPERIMENTAL STUDY OF THE INSTABILITIES (*)

I. JÁNOSSY (**), P. PIERANSKI and E. GUYON

Laboratoire de Physique des Solides, Université Paris-Sud, 91405 Orsay, France

(*Reçu le 17 mars 1976, accepté le 17 mai 1976*)

Résumé. — On discute expérimentalement les modes d'instabilités hydrodynamiques obtenues lorsqu'un film nématique est placé dans un écoulement de Poiseuille plan tel que le directeur soit perpendiculaire à la vitesse et au gradient de vitesse.

On peut obtenir des instabilités homogènes (distorsion uniforme dans le plan des plaques limites) avec ou sans écoulement transverse induit. Les valeurs des seuils sont comparées avec l'analyse théorique donnée dans l'article suivant.

L'effet d'écoulements alternatifs et celui de champs extérieurs appliqués sur la nature des modes et la valeur des seuils sont étudiés. On s'intéresse en particulier à la transition avec le mode en rouleaux. Comme aucune théorie n'existe actuellement sur ces problèmes, l'analyse est faite en référence avec le problème de cisaillement simple bien que des différences importantes existent.

Abstract. — This work discusses experimentally the hydrodynamic instabilities of an oriented nematic film contained in a plane Poiseuille flow cell such that the director is initially perpendicular to the velocity and velocity gradient.

Homogeneous instabilities having a uniform distortion in the plane of the boundary plates are obtained with or without distortion of the flow profile. The thresholds are analysed and compared with the theoretical analysis given in the following paper.

The effect of alternating flow and of the application of external fields on the nature of the mode and on the threshold is analyzed with attention to the transition from the homogeneous to roll instabilities. No detailed theory exists for these problems and the analysis is carried with reference to the simple shear flow case although marked differences are observed.

1. **Introduction.** — In a previous article [1] (hereafter called I) we have given an initial qualitative description of some instabilities obtained when a nematic liquid crystal is inserted in a plane Poiseuille flow cell with the initial director alignment at right angles to the plane of the velocity (Geometry of Fig. 1*a*). We wish to complement this study by semi-quantitative results, both experimental and theoretical, which lead to a better understanding of the homogeneous instability and to a closer contact with the corresponding shear flow problem [2]. We will also present some additional data on the convective modes although the theory of these modes has yet to be developed.

A semiquantitative analysis of both shear and Poiseuille problems has been given, based on consideration of the balance between elastic torques magnetic, electric and hydrodynamic (including the effect of *hydrodynamic focusing* effects in the case of a heterogeneous distortion). This one dimensional model neglects the variation of properties across the cell thickness and in particular it fails to predict the exact threshold as well as the detailed structure in the plane of the cell (wave length of convective rolls in the inhomogeneous case, existence of domains in the homogeneous one). Recently, a detailed two dimensional analysis of the shear flow instability problem has been given [3] which extends the previous treatment and is in excellent agreement with experiments in this

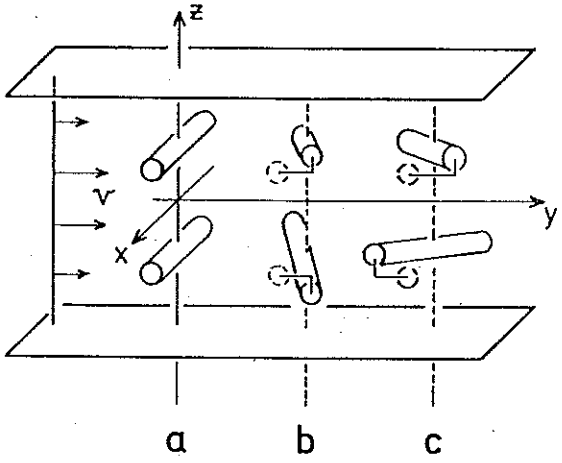

FIG. 1. — *a*) Director configuration in the Poiseuille flow cell in small enough flows. *b*) Is an even function of z in twist, odd in splay. *c*) Is an odd function of z in twist, even in splay.

(*) Ce travail a bénéficié de l'aide de l'A.T.P. *Instabilités dans les fluides et plasmas* du C.N.R.S.

(**) On leave from Central Research Institute for Physics, Budapest, Hungary.

geometry. A similar study has been undertaken in the Poiseuille case and will be described in the following article by Manneville and Dubois-Violette (II in the following).

The problem is more complex here because the shear flow rate

$$s = \frac{\partial v_y}{\partial z} = s' z$$

is a function of the distance to the boundary plates perpendicular to z. A simple approach is to consider that the distortion develops first near the boundary plates where the shear is largest. However, interference between these solutions due to elastic as well as flow coupling needs to be considered and the z dependence effect is essential to the description.

In chapter 2, we discuss the original features in the experimental description of the flow cell and of the pressure measurement and control.
the theoretical description for the homogeneous instability.

Considerations of symmetry of the solutions will shed some light on the more complex modes not yet studied theoretically. In the same part 3, we discuss the experimental occurrence of several homogeneous instability modes. Part 4 discusses the effect of alternating flows as well as of electric and magnetic field. Despite the richness of the instability modes obtained, much remains to be done before a quantitative understanding of the convective modes can be obtained.

2. **Apparatus.** — 2.1 FLOW CELL. — The flow cell is made up of two parallel plates of organic glass (altuglass) P_1 and P_2 separated by uniform metallic wires F (diameter $d = 0.2$ mm), stretched along the length of the cell (Fig. 2); the width of the cell l has been varied between 1 and 20 mm. The wires also limit the transverse flows. In the upper plate two cavities C have been milled near the ends. They act as reservoirs for the L.C. supply in the cell and also serve to prevent the formation of a meniscus inside the flow cell. The volumes are partially filled with L.C. (M.B.B.A., a room temperature nematic, was used throughout the experiment). The flow is induced by applying a pressure difference Δp between the small tubes T connected to the reservoirs. The size of the reservoirs is large enough to allow us to be able to neglect the pressure differential due to the difference of levels in comparison with Δp. The planar alignment of the nematic (n perpendicular to the flow axis y) is obtained by polishing the inner plates or by coating them with a semitransparent conducting Au film deposited under oblique incidence if conducting electrodes are needed. The cell is attached rigidly by two sets of screws and sealed with epoxy.

2.2 PRESSURE MEASUREMENT AND REGULATION. — A typical threshold for homogeneous instabilities for the geometry used (length of the cell $L = 108$ mm; $d = 0.2$ mm) corresponds to $\Delta p \sim 1.5$ mm H_2O. The threshold can be 10 to 50 times larger if a stabilizing magnetic field is used or in a large enough frequency alternating flow (the sign of the pressure difference is inverted with a frequency f from 10^{-3} to 10 Hz). In order to produce and stabilize the small pressures involved with an accuracy of the order of 1 %, we have developed the following device with four pressure stages (Fig. 3).

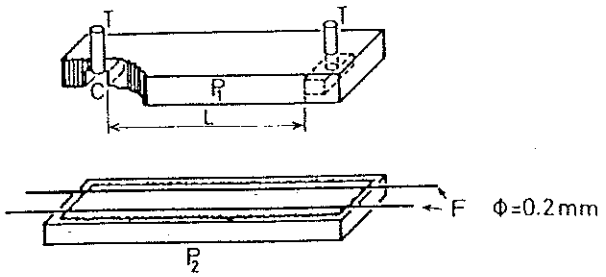

FIG. 2. — Schematic of the Poiseuille cell. The directions correspond to those in the first figure.

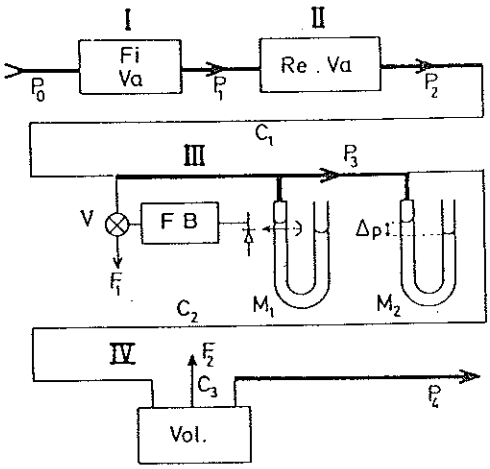

FIG. 3. — Pressure regulation and reading equipment.

The first stage I uses a filter and a pressure reducing valve (Fi, Va) to decrease the air pressure from a pressure tank to an overpressure $P_1 \sim 1$ atm with an accuracy of 10 %.

The second stage II is a more accurate regulating valve (Re, Va) (Gec Elliott Automation 40-2) which lowers the pressure to a value P_2 which can be regulated from 1 to 100 cm H_2O.

The third stage III is the crucial one : A thin tube C_1 (length ~ 50 cm, diameter 5 mm) connects the second stage to a needle valve V opened to the outside. The opening of the needle valve is automatically regulated as a function of the pressure P_3 at the entrance of the valve (the pressure head P_2-P_3 is obtained from the value of the length of C_1 and the opening of V).

The pressure P_3 is read with a differential manometer with an accuracy of 0.1 mm. The pressure is regulated using an independent oil manometer. The

oil level is kept accurately constant using a system with a photocell and a light source facing each other and placed against one arm of the manometer [4].

As the oil level rises above that of the light beam and photocell, the cylindrical lens formed focuses light on the photocell. This causes an increase of the photoelectric current — the error signal — used to control the opening of the valve via a feedback system (F.B.).

In practice a direct action of the amplified signal to control the motor opening the valve is not very convenient : there is always a small dead zone in the rotation of the valve; the valve will only react for a minimum value of the photodiode signal. We have developed an electronic circuit where the motor controling the valve is subjected to a permanent alternating motion by applying a voltage U during a time t^+ and $-U$ during a time t^-. The period $t = t^+ + t^-$ and U can be adjusted to optimize the response time. The electronic circuit, between the photodiode and a power amplifier which delivers the voltage U, perform the following function : it chops the unequal time intervals t^- and t^+ which are such that $(t^- - t^+)$ is proportional to the error voltage read on the photodiode [5]. The system developed is free from all the disadvantages of the direct command of the motor of the valve by the error signal and gives an excellent long term stability.

The fourth stage IV : In order to increase the sensitivity of the reading of P_3 we have developed a simple *pressure divider*. The pressure P_3 is applied to a large reservoir through a long thin tubing C_2. A leak (F_2) is produced by connecting the reservoir with the outside through a thin open tube C_3 of the same diameter. The overpressure P_4 in the buffer reservoir is a small fraction of the overpressure P_3. An estimate of the ratio P_3/P_4 is obtained from the ratio of the lengths of the tube C_2 over C_3. However, this is not very accurate and a direct calibration (showing deviations from linearity) has been used. The pressure P_4 (typically between 0 and 10 cm H_2O) is applied to the flow cell and can be regulated and read through the P_3 stage with an accuracy of 5 %.

3. **Homogeneous instability** (corresponds to P_{1_A} in ref. [1]). — 3.1 INTRODUCTION. — We consider the case of a dc flow in the absence of external fields. The flow can be applied for a time sufficiently long along one direction (frequency $f \sim 10^{-2}$ to 10^{-3} Hz) so that the maximum displacement of the liquid $D = v_m/f$ is larger than the characteristic dimensions (width of the cell l, thickness $d(\ll l)$). When the pressure gradient G, measured by $\Delta p = GL$ and proportional to the maximum velocity v_m, is increased, the nematic becomes distorted above a critical threshold Δp_c. Just above threshold, the distortion characterized by the polar angles θ, φ defined below, is homogeneous across the width of the cell.

$$\mathbf{n} : n_x = 1 ; \qquad n_y = \varphi ; \qquad n_z = 0$$

It can be controlled by the rotation Φ (associated with $\overline{\varphi}$) and lateral displacement ($\overline{\theta}$) of the conoscopic image formed in convergent monochromatic light incident on the cell ($\overline{\varphi}$ and $\overline{\theta}$ are averages across thickness). Another important factor is the finite angle Ψ of the flow, measured in the central portion of the cell, with the y axis when distortion is present. The angle is measured from microscopic observation of the motion of dust particles introduced in the L.C. It is found in practice that, above the threshold, the only modification of the conoscopic image from the classical double set of hyperbola obtained for a planar sample is an overall rotation. Typical experimental results are given on figures 4 and 5.

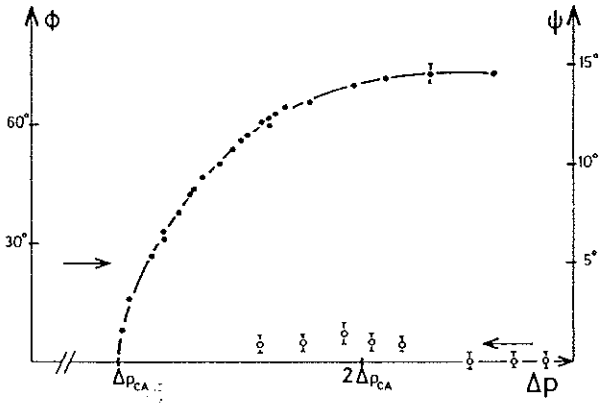

FIG. 4. — Variation of the twist distortion (measured by φ) above threshold Δp_{c_A} for the homogeneous instability mode A (the angle of the flow lines with y, Ψ, is practically zero everywhere).

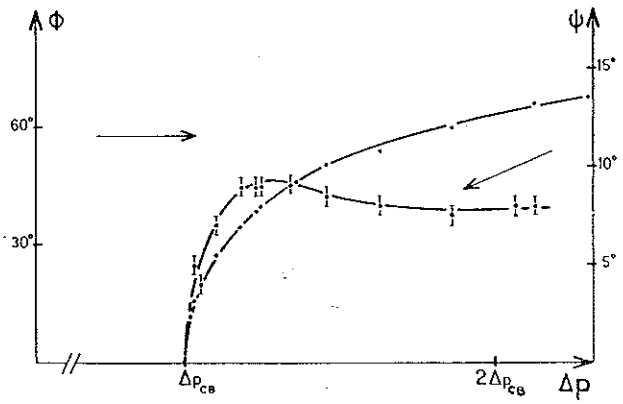

FIG. 5. — Same variations as in figure 4 for homogeneous mode B (Ψ is different from zero above threshold Δp_{c_B}).

3.2 MODEL. — The experiments and model developed here apply to materials such that the two hydrodynamic torques α_2 and α_3 are negative. This is the case when the coupling of the torque components due to fluctuating distortions n_z, n_y $\{(n_y), (n_z) \ll 1\}$ is destabilizing. The effect is acting against the stabilizing influence of the twist (K_2) and splay (K_1) elasticity. In addition we include the effect of a transverse flow $v_x(z)$ due to the component

$$\partial \sigma_{zx}/\partial z$$

of the Leslie-Ericksen stress tensor.

The unperturbed velocity profile is given by (origin of the coordinates midway between the plates) :

$$v_y^0(z) = \frac{G}{2\,\eta_a}\left(\left(\frac{d}{2}\right)^2 - z^2\right) \qquad (1)$$

and the shear rate by

$$s(z) = \frac{\partial v_y^0}{\partial z} = -\frac{G}{\eta_a} z = s' z \qquad (2)$$

we deduce the equations governing a fluctuation from those of the simple shear flow problem [3].

1) Torque equations : they are unchanged

$$-K_1 \frac{\partial^2 n_z}{\partial z^2} + \alpha_3 \frac{\partial v_x}{\partial z} + \alpha_3 s n_y = 0 \qquad (3.1)$$

$$K_2 \frac{\partial^2 n_y}{\partial z^2} - \alpha_2 s n_z = 0\,. \qquad (3.2)$$

2) Force equation : we must take into account the spatial variation of $s(z)$ in $\partial\sigma_{zx}/\partial z$; this gives

$$\eta_B \frac{\partial^2 v_x}{\partial z^2} + (\eta_b - \eta_a)\frac{\partial}{\partial z}(s n_y) = 0\,. \qquad (3.3)$$

The consideration of instability mechanisms described in ref. [2, 3] allows one to distinguish two types of distortion [1]

T) $n_y(-z) = n_y(z)$ and $n_z(-z) = -n_z(z)$

which involves an average *twist* over the thickness.

S) $n_y(-z) = -n_y(z)$ and $n_z(-z) = n_z(z)$

which involves an average *splay*.

This property is already apparent in eq. (3.2). In addition, from eq. (3.1) and (3.3), we deduce that v_x and n_y have the same parity. Moreover, we may consider the most general instability mode where the velocity fluctuations v_y and v_z and the pressure fluctuation no longer vanish. Using the continuity equation

$$\partial_x v_x + \partial_y v_y + \partial_z v_z = 0\,,$$

we deduce that v_y has the same parity as v_x or n_y, and v_z that of n_z. This result is of course compatible with the whole set of equations that may be adapted from the simple shear flow problem (ref. [3], appendix A).

A complete solution of the system (3.1) to (3.3) taking into account boundary conditions

$$n_y = n_z = v_x = 0 \qquad \text{at} \qquad z = \pm\frac{d}{2} \qquad (3.4)$$

is developed in 2.

Let us give a simplified description of the solution. Equation (3.3) describes a transverse flow effect, coupling the distortion of $\mathbf{n}$ in the xy plane to a deflection of the flow line along the x axis. By reinserting the variation of $v_x(z)$ in equation (3.1), one obtains a term linear in shear which renormalizes the α_3 term. If we neglect this renormalization which is tantamount to neglecting the transverse flow (such a solution can in fact be produced experimentally) [7, 8] we obtain the simple set

$$-K_1 \frac{\partial^2 n_z}{\partial z^2} + \alpha_3 s n_y = 0 \qquad (3.5)$$

$$K_2 \frac{\partial^2 n_z}{\partial z^2} - \alpha_2 s n_z = 0\,. \qquad (3.6)$$

Using the reduced variables $\tilde{n}_y = n_y$

$$\tilde{n}_z = \left\{\frac{K_1\,\alpha_2}{K_2\,\alpha_3}\right\}^{1/2} n_z$$

we get the symmetrical equations

$$\begin{cases} D\dfrac{\partial^2 \tilde{n}_z}{\partial z^2} - s' z \tilde{n}_y = 0 & (3.7) \\[2ex] D\dfrac{\partial^2 \tilde{n}_y}{\partial z^2} - s' z \tilde{n}_z = 0 & (3.8) \end{cases}$$

with a diffusivity of orientation

$$D_{\mathrm{cm^2/s}} = \left\{\frac{K_1\,K_2}{\alpha_2\,\alpha_3}\right\}^{1/2}$$

by addition and substraction, we get the decoupled equations

$$\begin{cases} D\dfrac{\partial^2 u}{\partial z^2} - s' z u = 0 & (3.9) \\[2ex] D\dfrac{\partial^2 v}{\partial z^2} + s' z v = 0 & (3.10) \end{cases}$$

where $u = \tilde{n}_y + \tilde{n}_z$, $v = \tilde{n}_y - \tilde{n}_z$.

The eigenvalue problems with the boundary conditions (3.4) are somewhat similar to Schrödinger equations with a variable potential well $\pm s' z/D$ (Fig. 6) and an eigenvalue = 0. We have obtained a numerical solution of the two equivalent equations (3.9), (3.10). The lowest eigenvalue is given by an Ericksen number characterizing the critical flow rate

$$\mathcal{E}r_c = \frac{G}{\eta_a}\left\{\frac{\alpha_2\,\alpha_3}{K_1\,K_2}\right\}^{1/2}\left\{\frac{d}{2}\right\}^3 = 12.8\,. \qquad (3.11)$$

The corresponding eigenfunctions localized near the bottom of the potential well are given in the figure 6. From the functions u, v one can construct two solutions for the distortion. The first one, given on the bottom of the figure 6, is antisymmetric in the splay

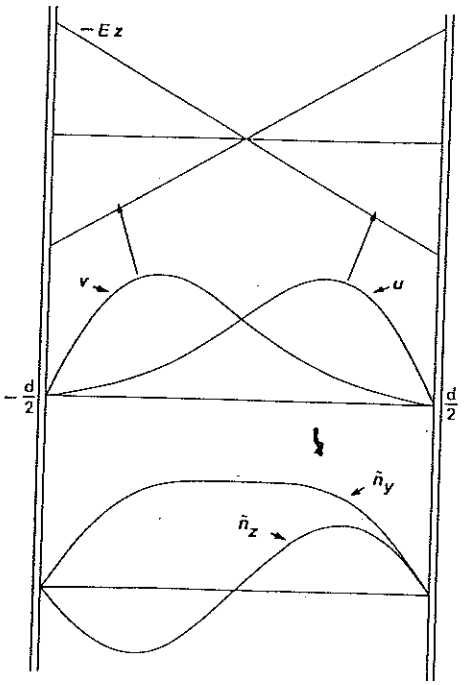

FIG. 6. — The solutions u, v of the eigenvalue equations (3.9)-(3.10) for the two possible forms $\mp Ez$ ($E = s'/D$) and one of the possible solutions for n_y and n_z (the one even in $n_y(z)$, which is obtained experimentally).

variable ($n_z(-z) = -n_z(z)$) and symmetric in twist. Another equally probable solution is symmetric in splay and antisymmetric in twist.

In experiments dealing with very wide cells, the first one is found to be more stable. The difference comes from the neglect of the flow coupling in this analysis : A transverse flow $v_x(z)$ symmetric in z is coupled with the twist solution symmetric in z.

The exact solution given in 2 includes the effect of transverse flow. Manneville and Dubois-Violette use in the following variables

$$N_z = \tilde{n}_z\,, \qquad N_y = \tilde{n}_y(\eta_a/\eta_b)^{1/2}$$

and an Ericksen number

$$\mathrm{Er} = \varepsilon r(\eta_a/\eta_b)^{1/2}\,.$$

The dependence of the critical threshold Er_c with (η_a/η_b) is given for both the average twist (T) and average splay (S) mode in figure 4 (II).

The analysis of II reduces exactly to our in the limit $\eta_a/\eta_b = 1$. In this case, the thresholds for the S and T solutions are the same. Note that in this limit the transverse flow disappears [6]. (The viscosity in the xy plane becomes also isotropic.)

3.3 EXPERIMENTS. — The solution (3.1) never applies exactly to the experimental condition as it neglects the effect of lateral boundary conditions which limit the transverse flow.

We discuss first experiments done using relatively wide cells ($l \sim 10$ mm, $d = 200$ μ). Interesting effects associated with the finite width will be discussed next.

Two instability modes are obtained which are characterized by the absence (A), or the presence (B) of transverse flows [13].

Regime A. — In figure 4, we have plotted the rotation angle Φ as a function of Δp. In this mode, φ does not vary across the length of the cell except possibly near the ends where the flow pattern is ill defined. Starting from large Δp, we see that φ is close to $\pi/2$. The director is everywhere nearly in the plane of the flow. The effect of the splay is limited to an angle θ_m with the flow axis, such that $\mathrm{tg}^2\,\theta_m = \alpha_3/\alpha_2$. This is however an antisymmetric contribution across d and the conoscopic image remains centered around the z axis. As the flow rate is reduced, θ decreases and vanishes for a critical pressure variation Δp_{cA}. Note the parabolic and continuous variation of Φ near threshold. This is characteristic of the second order mean field transition. On the same figure, we have, plotted the angle Ψ of the flow with y, determined from the motion of dust particles. No appreciable transverse flow is observed.

Regime B. — Increasing the pressure from zero, another possible solution is obtained which is shown on figure 5. Above a critical value Δp_{cB}, an average twist distortion θ develops as in the previous case.

An original feature of this solution is the existence of a transverse flow, characterized by a finite angle Ψ, above Δp_{cB}. The maximum value of Ψ around $\Phi = 45°$ is easily understood if one refers to our previous study [6] of transverse flows where the uniform orientation of the nematic in a Poiseuille flow cell was obtained by applying a large magnetic field at an angle φ with the flow axis. It was found, and explained, that the flow is deflected towards the direction of the director, due to the effect of the variable shear across thickness, and that a maximum deflection angle $\Psi \sim 10°$ was obtained around an oblique orientation of 45° as in this study.

A quantitative comparison between the two regimes lead to the following results.

— Regime B appears to be more stable than regime A for small distortions (typically $\Phi < 45°$) and has a smaller threshold.

This is why regime B is obtained by applying progressively larger Δp. However, in the case of large distortions, regime A is the most stable one and leads to a larger distortion φ for the same Δp.

In figure 7, we have indicated the variation of Φ obtained for decreasing values of Δp. Between two points of measurements, a very long time was kept (typically 1 hour). The discontinuous decrease of Φ is associated with the onset of mode B. However, as the time constant is so long, it is possible to describe the complete A and B curves as the time needed to obtain a new distortion value within the same regime is much shorter.

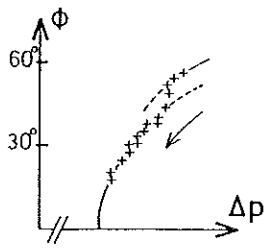

FIG. 7. — In this experiment the pressure difference Δp was reduced extremely slowly starting from a largely distorted state without transverse flow (solution A). For an intermediate pressure value another branch is reached which corresponds to the domain of stability of solution B (with transverse flow). Solution B is the most stable at threshold.

The existence of two solutions is consistent with the theoretical description.

Solution B corresponds to the solution (3.17) of II including the effect of transverse flow. A comparison between the experimental threshold and the theoretical one gives the following results for the experiment of figure 10 : $G_{exp} = 24.5$ cgs, corresponding to a theoretical evaluation, using equations (3.11) and (3.1) and the viscosity data given by Gähwiller [14], $G_{th} = 16.5$ cgs. The order of magnitude agreement is an indication of the overall validity of the model on the experiments.

The lack of quantitative agreement cannot be taken too seriously at the present stage as (3.11) involves a combination of viscous and elastic coefficients which are not known accurately from one set of experimental data to the next (for example the uncertainty on α_3 is of the order of 50 %).

Solution A can be understood if one considers the possibility of a pressure gradient term $\partial p/\partial x$ across the width of the cell which compensates the d.c. flow across the cell. This is possible for the solution involving an average twist ($n_y(z)$ even in z) obtained experimentally, where the velocity $v_x(z)$ variation is also even in z (for a type S solution where $v_x(z)$ is odd in z there is a possibility of transverse closed flow loops as obtained in the corresponding shear flow problem).

The solution of this problem is obtained by cancelling the contribution of the transverse flow (see form (3.11)). It clearly leads to a higher threshold than B. However a correct solution of this problem should clearly imply a discussion of the x dependence and on the side boundary effects, and the quantitative comparison cannot be pursed in the present stage.

Domains. — In our discussion of mode B we have not yet mentioned the very spectacular formation of regular domains along the length of the cell. The twist φ is uniform within one domain but changes sign rapidly as one crosses the narrow twist wall separating two domains. A photograph showing the optical contrast due to the different diffusion of light between domains was given in I, Fig. 4. Very regular structures can be produced if the instability is produced in the presence of a transverse magnetic field which limits the effect of defects due to surface misalignment. The very long time needed before the regular structure is obtained (whose effect was already obvious in the discussion of previous paragraph), arises from the fact that the creation of domains involves a diffusion of orientation over very large distances.

The wavelength of the domains, λ, is an increasing function of the width l and varies roughly linearly with it :

For cells of width $l = 5$; 10 ; 20 mm, we have found $\lambda = 3.1$; 4.3 ; 8.6 mm. (In fact, the characteristic time is so long, that the quantitative results must be taken with some care as they do not necessarily represent final equilibrium states.)

A possible mechanism for the description of the walls can be obtained from consideration of figure 8, giving schematically the velocity distribution in a frame moving with the velocity v_m.

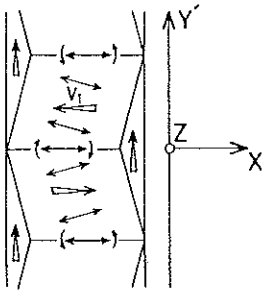

FIG. 8. — In a frame of reference $XY'Z$ moving at the velocity of the flow in the central portion of the cell the additional flow (↕) due to transverse forces is seen and cause a slightly backward motion of the walls (// to x) separating domains of opposite average twist.

The formation of domains allows the development of a transverse velocity v_T in a limited geometry. The triangular shapes which can be seen in the figure 8 insure the continuity of the velocity from one domain to the next. The sign of the z component of the hydrodynamic torques due to the gradient $\partial v_T/\partial y$ is the same in both domains 1 and 2. Consequently the domain of existence of 1 increases and a backward relative motion of the domain walls is obtained. Indeed it is observed experimentally that the motion of the walls is slower that the flow velocity in the central flow field. We have also followed the motion of small particles. When a particle, in relative motion with respect to a wall, crosses it, its transverse motion changes sign quite discontinuously.

Narrow cells. — In cells typically narrower than $l = 3$ mm, the formation of domains and the solution B are strongly inhibited. In these cells it is possible to produce in a quite equivalent fashion the average twist (type 1) and average splay (type 2) solutions. By applying temporarily an oblique magnetic field (H in the plane perpendicular to the flow) in the presence of the flow, one induces a splay of **n** in the cell. If the

pressure gradient is larger than the critical value, the splay solution (n_y odd and n_z even functions of z) of the Poiseuille problem remains after the field is suppressed. It appears that the threshold of this solution and that of the twist one are very close for a given cell. This is consistent with the simplified solutions obtained when one neglects the transverse flow. The splay solution should however involve some flow (v_x has the same odd parity as n_y and a transverse pressure cannot cancel v_x completely).

As a conclusion of this discussion we want to point out the limit of applicability of the model to the experimental situation and the need for a (apparently complex) solution where long range two dimensional effects in the plane of the film are considered.

4. **Alternating flow and field effects.** — An original feature in the study of instabilities in nematics is the possibility of control by application of electric and magnetic fields. We have used both a stabilizing magnetic field H_x acting on n_y and n_z, and a stabilizing electric field E_z acting on n_z.

The effect of the field can be introduced in the definition of the relaxation time constants for n_y and n_z.

The effect of H and f on the threshold have been considered at the same time on the graphic construction of figure 9.

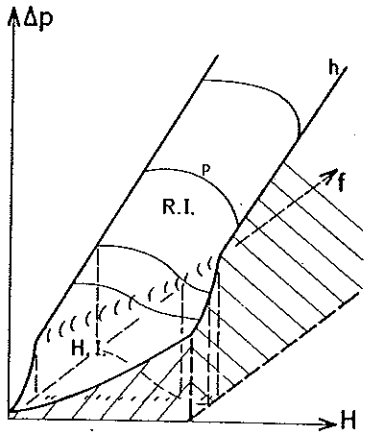

FIG. 9. — 3 D diagram indicating the limit of stability of the homogeneous (H.I.) and roll (R.I.) instabilities; the constant Δp curves (p) and magnetic field curves (h) were obtained experimentally. The d.c. threshold curve ($f = 0$) agrees quantitatively with the analysis of (I) (see 3-3 of I). The unstable region is above the surface.

4.1 FREQUENCY EFFECT ($H = E = 0$). — Let us first consider the situation in the absence of fields (Fig. 10). The threshold of the homogeneous instability (H.I.) increases first with frequency. This is simple to understand as the effect of a finite time for the growth of an instability should increase the effective threshold.

However for frequencies typically larger than 0.15 Hz another mode (which will be referred as R.I.) is obtained at threshold, where convective rolls along the flow axis are formed. A qualitative description of

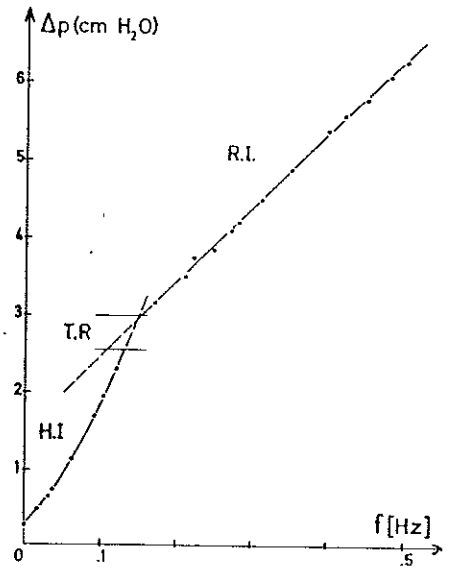

FIG. 10. — Gives in more detail a constant field curve (for $H = 0$) for a 200 μ thick, 10.8 cm long flow cell. In the transition regime (TR) between the H.I. and R.I. ones, both modes can be found at the same time in different regions of the cell.

the rolls has been given in I and will only be recalled briefly. The mode obtained at threshold is even in n_y and odd in n_z just as the homogeneous one (see Fig. 8 of I).

The rolls involve a periodic distortion $n_y(x)$ of **n** across the rolls. The effect of the distortion in inducing hydrodynamic focalization terms and new destabilizing mechanisms has been analysed in detail in the corresponding shear flow problems [2, 3].

The wavelength of the rolls is of the order of d for low Δp and decreases as Δp increases (typically as $\Delta p^{-1/2}$). This feature indicates that the distortion is localized in each half plane near the limiting plates and suggests the formation of two sets of convective rolls near the plates. This result is consistent with the fact that the velocity $v_z(x)$ should have the same parity as $n_z(x)$ (see table of II) and be zero in the central plane. The convective rolls formed near one plate do not extend to the opposite one and do not contribute to the coupling between the two solutions. However an elastic coupling is still present between the distortions present in the two superficial sheaths where the shear is largest.

The convective [10] flow has been detected directly from the observation of the motion of dust particles undergoing spiral motions in the flow.

As the sign of the flow is inverted, the distortion n_y changes sign but not n_z. This result was obtained by optical observation of the focal lines which are formed due to the modulation $n_z(x)$. The lines do not change position over each half period. In the corresponding shear flow problem [2] such a regime was called Y mode. It is not clear whether such a simple description of the dynamic interplay of n_y and n_z is sufficient here.

One can characterize the threshold from the occurrence of the diffraction pattern of a wide parallel

monochromatic beam incident on the sample. A photocell linear in response is coupled with a X – t recorder and the onset of the transition is detected accurately.

4.2 MAGNETIC FIELD. — Coming back to figure 9, we analyse the additional effect of an applied field. A curve similar to that of figure 10 but obtained in a field $H_x = 2\,750$ G is given (h). It also shows the existence of a H.I. domain for small frequencies and a R.I. one for larger ones. Note however that the thresholds Δp_c are larger than for $H = 0$ due to the stabilizing influence of H. We may also note that the domain of existence of the H.I. does not appear to decrease as H increases unlike the shear flow case. In fact the limit frequency $f \approx 0.15$ Hz (for $d = 200$ μ) is the same on both $H = 0$ and 2 750 G curves. The variation of threshold with fields at $f = 0$ is discussed in II. It is shown that the experimental variation of $\Delta p_c(H)$ expressed in terms of the Ericksen number agrees with theoretical predictions (see figure 9 of II).

The critical surface can be also mapped by studying the variation of the critical frequency versus H keeping Δp constant (curves p). The curves also display the change of regime between RI and HI. It may look surprising that the homogeneous instability develops in this case for large values of H. One could have expected that the stabilizing effect of H, which is independent of the spatial variation of $\mathbf{n}$, overcomes that of the elasticity and tends to favor the formation of rolls if the destabilizing mechanisms are more effective in this case. The detailed analysis of the forces in this case remains to be done. We also note that, as H increases at constant Δp, the wavelength of the rolls tends to increase slightly (by 10 % from $H = 0$ to the transition regime). This is due to the effect of the corresponding decrease of f ; λ is never very large as compared with the magnetic coherence length and the elastic effect can never been neglected unlike the shear flow case.

4.3 ELECTRIC FIELD. — The effect of an electric field applied between two transparent conducting electrodes deposited on the boundary plates has been used extensively to control the type of instability mode present at threshold.

The figure 11 presents the limit of stability of convective solutions in coordinates V, T^{-1}. Each curve corresponds to a given pressure difference and the magnetic field is kept constant through the experiment. The characteristic S shape solution has already been obtained in other instability problems in nematics [2], [11] and defines two types of convective solutions.

For $V < V_{cu}$, where V_{cu} refers to the cusp of the curve, the instability observed at frequencies below the critical corresponds to that discussed above for $V = 0$.

Above V_{cu}, the instability mode appears to be characterized by the following features :

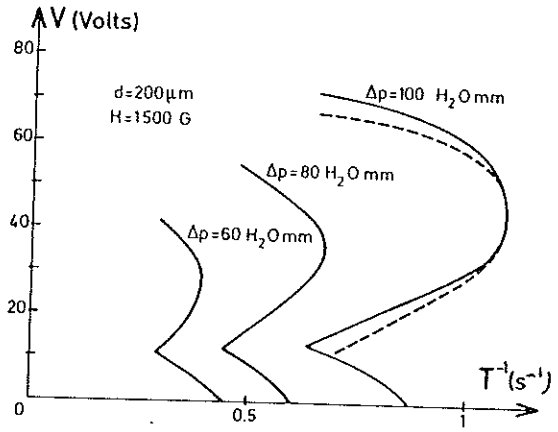

FIG. 11. — Instability thresholds for roll instabilities obtained in AC flow. Constant Δp curves are given. A destabilizing electric field along $z(E = V/d)$ has been applied. Note the hysteretic effect shown on curve $\Delta p = 100$ mm. The broken line curve was obtained in decreasing voltages.

— Zero average twist and non zero average splay across thickness.

— Periodic modulation of n_y and n_z along x (across the rolls).

— Wavelength of the rolls relatively independent of voltage (the change of wavelength between the two convective regimes can be quite large as the wavelength in the previous case could be much smaller than d for large frequencies and Δp).

— The velocity $v_z(x)$ is an even function of z (same parity as $n_z(z)$). This point is consistent with the previous one as it indicates the possibility of simple convective loops across the cell, whose size is controlled by the cell thickness.

— The time dependent properties of this mode are consistent with a Z type solution, as introduced in shear flow problem [2], where only n_z changes sign over each period. The conditions of existence of this solution as well as the dynamic behaviour are connected with the fact that, as E increases, T_z/T_y decreases, which makes the n_z relaxation easier.

The characteristics of this mode (refered as II) are very similar to those of the mode P_{2B} discussed in I and which can be produced by application of a value Δp sufficiently larger than the threshold value.

The cusp shape can be revealed in a single experiment at a constant frequency $f = 0.5$ H_z (keeping $\Delta p = 80$ mm H_2O constant).

Figure 12 gives schematically the recording of the intensity of the lowest order diffracted peak of a parallel laser beam. For $E = 0$, Δp is larger than the critical value and the light intensity is finite.

As E is increased towards a first critical value E_{I0}, the intensity decreases regularly to zero (indicative of a second order transition on the branch I). The intermediate stable domain corresponds to the inside of the cusp. At a critical value E_{0II}, a diffraction pattern is obtained again up to a value E_{II0}. This is the domain

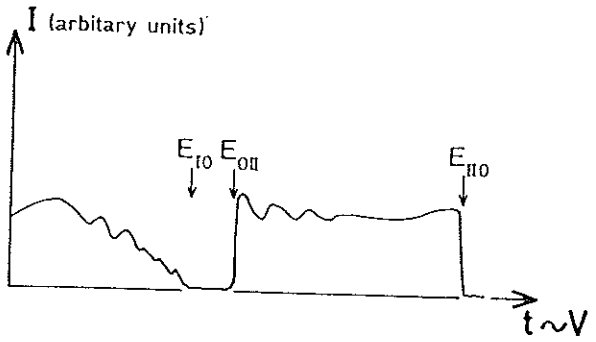

FIG. 12. — The photocell detection of the diffraction pattern of a monochromatic beam by the convective structure. The pressure head was kept constant and the electric field E was increased continuously. A time modulation of the intensity has been obtained systematically and is not understood.

of existence of solution II. We note that the transitions at the two fields are very sharp and, in fact, a hysteretic behaviour indicated by the existence of two threshold curves, depending on whether the field is increased or decreased (see the full and broken lines in figure 11) is obtained. The effect may be connected with the fact that, for large electric fields, the distortion of the electric field pattern within the L.C. is coupled with that of **n**.

5. **Conclusion.** — In this study, we have extended our qualitative description of the Poiseuille flow instabilities in nematics. If one compares with the isotropic case [12], the remarkable features here are : the existence of instabilities for very slow flows (Reynolds number $\sim 10^{-2}$) ; existence of linear instability modes just above threshold ; a rich variety of convective and non convective structures. Some problems have been solved but those involving a consideration of the structure within the plane of the cell remain to be treated.

From the point of view of *liquid crystallographers* this problem may not appear as of primary urgency. Many problems met in such a study can be carried out in the simpler shear flow case ; the viscoelastic behaviour can also be studied on the basis of simple model experiments. Nevertheless, some challenging problems original to this study are left open. These include the important role of the transverse flows which conditions the domain structure in the homogeneous solution and the interference between the two instabilities nucleated near the surface layers and interacting via elasticity and hydrodynamic coupling. Finally, the simplicity of the preparation of this experiment and the spectacular vizualisation of the diffraction pattern by the convection rolls makes it a remarkable pedagogical tool to demonstrate instabilities. All these comments concern linear problems. In the wide open field of non linear instabilities and approach to chaos, the Poiseuille flow problem may also be a good candidate (in particular using the diffraction pattern to analyze the growth of distortion).

References

[1] GUYON, E. and PIERANSKI, P., *J. Physique Colloq.* **36** (1975) C1-203.

[2] PIERANSKI, P. and GUYON, E., *Phys. Rev. A* **9** (1974) 404.

[3] MANNEVILLE, P. and DUBOIS-VIOLETTE, E., *J. Physique* **37** (1976) 285.

[4] ADKINS, C. J., A similar optical system has been proposed to control the helium pressure on a cryogenic bath. *J. Sci. Instrum.* **38** (1961) 305.

[5] PIERANSKI, P., A detailed description of the system can be found in the doctorat d'Etat, Orsay (1976).

[6] PIERANSKI, P. and GUYON, E., *Phys. Lett.* **49** (1974) 237.

[7] DE GENNES, P. G., Les Houches (1973) *Fluides Moléculaires* (édité par Balian, Weill. Gordon Breach) 1976, p. 397.

[8] GUYON, E., *In fluctuations, Instabilities and phase transitions* edited by T. Riste (Plenum Press) 1974, p. 303.

[9] MANNEVILLE, P. and DUBOIS-VIOLETTE, E., to be published.

[10] We may note that, although convective motions are involved in these instabilities, the flow enters only linearly as a coupling term between fluctuating variables. It does not enter into non linear (v∇) convective terms unlike the classical Benard (or Taylor) convective instabilities where the convective transfer of heat (or linear momentum) is the destabilizing mechanism.

[11] SMITH, I. W., GALERNE, Y., LAGERWALL, S. T., DUBOIS-VIOLETTE, E. and DURAND, G., *J. Physique Colloq.* **36** (1975) C1-1.

[12] For example ZAHN, J. P., TOOMRE, J., SPIEGEL, E. A. and GOUGH, D. O., *J. Fluid Mech.* **64** (1974) 319.

[13] In [1] we had characterized with indices A and B the flow solutions governed by the force $F_A = \partial\sigma_{zx}/\partial z$ (due to the variable shear across thickness in the Poiseuille problem) and by the force $F_B = \partial\sigma_{zx}/\partial x$ (due to the existence of a variable distortion across the width of the cell for the convective modes). A and B have different meaning here. Let us note that the difference between the modes associated with F_A and F_B in [1] was rather artificial as both forces are acting at the same time in the convection regime.

[14] GÄHWILLER, Ch., *Mol. Cryst. Liq. Cryst.* **20** (1973) 301.